Magnetic properties of graphite irradiated with MeV ions

M. A. Ramos,[1,*] J. Barzola-Quiquia,[2] P. Esquinazi,[2,†] A. Muñoz-Martin,[1] A. Climent-Font,[1] and M. García-Hernández[3]
[1]*CMAM and Instituto de Ciencia de Materiales "Nicolás Cabrera," Universidad Autónoma de Madrid, Cantoblanco, E-28049 Madrid, Spain*
[2]*Division of Superconductivity and Magnetism, Institut für Experimentelle Physik II, Universität Leipzig, Linnéstraße 5, D-04103 Leipzig, Germany*
[3]*Instituto de Ciencia de Materiales de Madrid, CSIC, Cantoblanco, E-28049 Madrid, Spain*
(Received 18 January 2010; revised manuscript received 13 April 2010; published 3 June 2010)

We have studied the change in the magnetic properties produced on highly oriented pyrolytic graphite samples by irradiation of H, C, and N ions in the mega-electron-volt energy range. The use of specially made sample holders for the magnetic measurements provided high reproducibility allowing us to obtain directly the irradiation effects without any corrections or subtractions. Our results show that three magnetic phenomena are triggered by the defects produced by the irradiation, namely, Curie-type paramagnetism, ferromagnetism and an anomalous paramagnetic state that appears as precursor of the magnetic ordered state. Using SRIM simulations to estimate the amount of vacancies produced by the irradiation, the Curie-type paramagnetic response indicates an effective Bohr magneton number per nominally produced vacancy $p=0.27\pm0.02\mu_B$. Direct measurements of the surface sample temperature during irradiation and the decrease in the (as-received) paramagnetic as well as ferromagnetic contributions after irradiation indicate that self-heating is one of the causes for small yield of ferromagnetism. Taking into account the hydrogen distribution in the virgin samples, the obtained results indicate that the induced ferromagnetism appears when the average vacancy distance is ~2 nm in the near surface region.

DOI: 10.1103/PhysRevB.81.214404 PACS number(s): 75.50.Dd, 81.05.uf, 61.80.−x, 71.55.Ak

I. INTRODUCTION

The introduction of defects in the graphite structure by ion-beam irradiation is an ideal method to test the influence of lattice defects, i.e. vacancies and carbon interstitials or other adatoms, on the magnetic properties of graphite. Ion irradiation allows us to minimize sample handling and to estimate quantitatively the produced defect density per graphene layer as a function of penetration depth within the graphite structure using well-known standard programs such as SRIM (the stopping and range of ions in matter[1,2]). Although the study of the irradiation effects in graphite was a major research area in the past, the influence of lattice defects in the magnetic properties was only noted through the increase in the spin density and the decrease in the Landau diamagnetic response.[3]

Till the end of the 1990s there was basically consensus that disorder in a graphite or other carbon-based structure produces a paramagnetic behavior due to the formation of nonbonding electrons (dangling bonds). *Ab initio* calculations indicate that a C adatom on a graphene sheet can have equilibrium positions with a finite magnetic moment on the order of $0.5\mu_B$.[4] This moment can be understood if we consider that the hybridization state is different for the two top C atoms attached to the C adatom and this last one, i.e. sp^2-sp^3 vs sp^2 hybridization, respectively. In this case half p_z electron of the C-adatom provides the $0.5\mu_B$. In Ref. 5 the magnetic state of a vacancy in a graphene sheet was analyzed. The results indicate that the vacancy undergoes a Jahn-Teller distortion leaving a dangling bond that is responsible for $1.04\mu_B$ magnetic moment. In recent years a further rich spectrum of magnetic states has been theoretically proposed for a single graphene layer as well as for the graphite structure, i.e. multigraphene, which includes from the pinning and switching of localized magnetic moments[6] to the description of magnetically ordered states (ferromagnetism) in a graphite structure with vacancies or hydrogen adatoms.[7–9] Recently published theoretical studies emphasize the role of vacancies, hydrogen partially saturated vacancies and divalent additions to trigger long-range ferromagnetic coupling in graphite or graphene mediated by the π electrons.[10]

A rather unexpected magnetic effect has been reported in Ref. 11, namely, inducing ferromagnetism or ferrimagnetism by proton irradiation at ~2 MeV energy and fluences below 10^{18} cm^{-2} on pure highly oriented pyrolytic graphite (HOPG) samples. This effect has been reproduced in further, similar irradiation studies[12,13] and also using carbon ions at much lower energies.[14,15] Results obtained in Ref. 13 indicated that the measured magnetic signal produced by the irradiation was mainly located in the first micrometer depth. If one assumes that the magnetism is solely due to the produced vacancies, SRIM simulations of the irradiation damage would indicate that the largest ferromagnetic *sample mass* one can produce with a single energy proton beam will be located at the first ~10-μm depth. This is because in this depth range the curve mean vacancy distance vs penetration depth is rather flat.[16] Following the estimates done in Ref. 7 based on the ferromagnetic contribution of coupled defects from the same sublattice of the graphene lattice, a mean distance between vacancies of $\sim 1.5, \ldots, 2$ nm would give a critical temperature of ~450 K in fair agreement with experimental observations.[13,14]

X-ray magnetic circular dichroism (XMCD) studies on proton-irradiated spots on carbon films showed that the magnetic order is correlated with the π electrons of carbon, ruling out the existence of magnetic impurity contributions.[17] Recently done XMCD studies on bulk graphite samples[18] not

only confirmed the magnetic polarization of the π electrons of carbon and its enhancement after irradiation but also indicate that the main ferromagnetic contribution in proton irradiated graphite is located at the first ~20 nm from the surface and that hydrogen plays also a role in the magnetic order, as was previously shown theoretically.[19] These last XMCD results[18] support the findings from a low-energy muon spin rotation (LEμSR) experiment on HOPG samples that indicate the existence of a ferromagnetic surface of ~15-nm thickness.[20] Further theoretical work showed that the magnetic coupling becomes weaker when the hydrogen-hydrogen distance increases, resulting in a decrease in the net magnetic moment.[7,21]

On the other hand, magnetic force microscopy, XMCD, and scanning transmission x-ray microscopy (STXM) measurements on irradiated spots indicate the existence of qualitatively different regions within a proton-irradiated spot and its surroundings.[22] Namely, a nonmagnetic conducting center surrounded by an insulatinglike magnetic ring embedded in the nominally nonmagnetic graphite matrix. Electron spin resonance (ESR) studies on proton-irradiated graphite showed the rise of a L1 line in addition to modified D1 and D2 lines attributed to the ordered and disordered graphite phases.[23] Recently published ESR studies on proton-irradiated HOPG samples at different fluences indicate the existence of metalliclike islands surrounded by insulatinglike magnetic regions[24] in agreement with previous findings.[22] It is therefore of interest to check whether direct magnetic-moment measurements triggered by the irradiation can reveal features compatible to this apparent phase separation.

All these results put also a main question on the way to trigger magnetically ordered state via ion irradiation in graphite. Namely, which is the range of parameters needed to trigger magnetic order through the generation of defects in the graphite structure? Following the theoretical estimates from Refs. 7, 9, and 10 one would expect that inducing a determined amount of vacancies in the graphite structure a magnetically ordered state should be obtained, independently whether this amount is at the near surface region or at 10-μm depth from the sample surface. However, if hydrogen plays a role, then there will be a dependence on the selected region since we know that the near surface region, i.e. the first micron, shows a much larger hydrogen concentration than deeper inside a HOPG sample.[25,26] Furthermore, we note that a systematic and quantitative study of the relationship between the vacancy number in the graphite structure produced by mega-electron-volt (MeV) ions and the different magnetic contributions was not yet thoroughly published in the literature.

Using new developed sample holders for superconducting quantum interference device (SQUID) and irradiation studies, high reproducibility has been achieved in the magnetic measurements allowing us to study in detail the temperature and magnetic field dependence of the magnetization of HOPG and its change after ion irradiation. In order to study heating effects during irradiation, in this work we also measured the sample surface temperature with an infrared camera. The irradiation has been done using protons, carbon, and nitrogen ions in the energy range between 1.2 and 25 MeV, which covers maximum penetration depths between ~1 and 460 μm from the sample surface. In this work we discuss three different magnetic responses induced through the defects produced by ion irradiation in an otherwise purely diamagnetic graphite.

The paper is organized as follows. In the next section we provide a short overview on the generation of defects by ion irradiation and implantation and we explain how we use the standard program to compute the induced defect density for the case of the graphite structure. In Sec. III we present in two sections the main experimental details concerning this study. In Sec. IV A we explain how we treat the measured data in order to characterize the magnetic effects induced by the ion irradiation. Secs. IV B–IV D show the used theoretical description to interpret the experimental data, especially the temperature dependence of the magnetic moment induced by ion irradiation. The experimental results are presented in Sec. V, which is divided in three sections taking into account different effects observed by the ion irradiation. The discussion and conclusion are presented in Secs. VI and VII, respectively.

II. SHORT REVIEW ON DEFECTS GENERATED BY ION IMPLANTATION AND IRRADIATION

A. Ion-beam irradiation and damage

Structural defects in solids are typically divided[27] into *point defects* and *extended defects*. Point defects can in turn be considered as intrinsic or extrinsic. Well-known examples of intrinsic point defects are vacancies (missing atoms in the lattice) and interstitials (atoms occupying nonlattice sites). Extrinsic point defects typically arise from foreign atoms or impurities. On the other hand, among extended defects we may mention dislocations or grain boundaries.

Among different methods of producing point defects, we will focus on ion-beam implantation and irradiation, currently also named ion-beam "modification,"[28] though electron or neutron irradiation could also be used. Nevertheless, ion irradiation can deposit quasi-instantaneously very high energy densities in matter, what is not feasible employing other irradiation methods such as high-power lasers. When an energetic ion impinges on a solid target, a very rapid transfer of energy from the ion to the target atoms is produced. The total rate of energy transfer can be many keV/μm of ion path. As a consequence, the original lattice structure becomes disordered (radiation damage), atoms leave the surface (sputtering), and the implanted ions remain buried at the end of their damage track (doping).The energy transfer occurs via several mechanisms with the dominant processes being excitation of electronic states or nuclear collisions between the incident ions and the target ions. In the case of metals and semiconductors, the radiation damage is almost entirely governed by the energy deposited in nuclear collisions. For insulators and high ion energies, electronic excitation would however dominate atomic displacements in the target material.[27]

Although damage from fast-neutrons irradiation has often been used in the past to study the case of graphite, there has been a gradual rise in interest in damage produced by electron and ion irradiation[29,30] for the reasons pointed out

above. In general, it is usually assumed that the dominant structural defects are the Frenkel-pair defects, i.e. a vacancy plus an interstitial atom, that may recombine or diffuse and form aggregates or clusters, as well as multivacancy defects (a recent review on radiation defects in graphite is found in Ref. 31). As a rule, the extent of radiation damage tends to be reduced if the exposure takes place at a higher flux or at higher temperature, or if some thermal annealing is allowed. Let us also mention that the technique of measuring positron annihilation lifetimes has been applied to graphite[15,32] in order to examine different multivacancy defects. In particular, the planar V_6 defect was found to be particularly stable and abundant in heavily neutron-irradiated graphite[32] and also near the surface in 70 keV C-ion irradiation experiments,[15] whereas single-vacancy and divacancy defects were distributed deeper in the sample.

B. Monte Carlo simulations: The SRIM programs

The analysis of the collision damage process induced by ion irradiation can be adequately investigated by computer simulation techniques, mainly through Monte Carlo methods. The simplification is usually made to consider the target material as amorphous, ignoring the possible periodic order of its atoms. In practice, there are little differences between the results obtained for amorphous or crystalline states of the same irradiated material, unless one is interested in specific features such as ion beam channeling in crystals. The most popular and widely used simulation method is called SRIM (stopping and range of ions in matter).[2] SRIM is indeed a group of programs, based on an earlier core program called TRIM (transport of ions in matter),[33] that is continuously upgraded and freely used. SRIM/TRIM programs employ a statistical Monte Carlo simulation method within a binary-collision approximation that calculates the stopping and range of ions into matter using a quantum mechanical treatment of ion-atom collisions. It is important, however, to stress that no evaluation is made of the thermal effects in the solid, especially the redistribution of lattice atoms or implanted ions by thermal- or vacancy-induced diffusions. This means that all the defect densities we obtain using the SRIM program should be taken as the maximum possible values.

By means of SRIM calculations, one can obtain the implanted-ion distribution after those sent ions have lost their energy and have stopped in the target sample, as well as the distribution as a function of depth for the vacancies produced along the ion track, among other data. For the case of a graphite sample, one finds that the reached ion range by light protons H^+ (for example, 38 μm at 2 MeV, 55 μm at 2.5 MeV, or 213 μm at 5.5 MeV) is much deeper than that by carbon ions (1.9 μm at 2 MeV or 20 μm at 25 MeV), as expected. The depth window where the irradiated ions remain implanted is very narrow. On the other hand, a relatively broad peak of vacancy density is always observed very close to the implantation range whereas a rather flat distribution of vacancies is generated in the track from the surface to that maximum in defect density and ion range, as can be seen in Fig. 1.

There are few direct comparisons between the calculated vacancy density from these computer simulations and the measured one after ion-irradiation experiments. We may mention nevertheless two recent studies conducted just in graphite. Three-dimensional hydrogen analysis done on irradiated micrometer size spots using 2.25 MeV H^+ ions on HOPG confirmed that the implanted H stays well located at the implanted sites, both laterally as well as in depth, in agreement with SRIM simulations and without having evidence of diffusion broadening along the implantation direction, i.e., the c axis.[25] On the other hand, clear evidence for lateral hydrogen diffusion due to thermal effects over large distances was also observed.[25] In Fig. 2b of Ref. 15, the depth distribution of vacancy-defects density produced by carbon ions at 70 keV was determined from positron annihilation experiments and found to agree reasonably well with the distribution obtained from SRIM simulations.

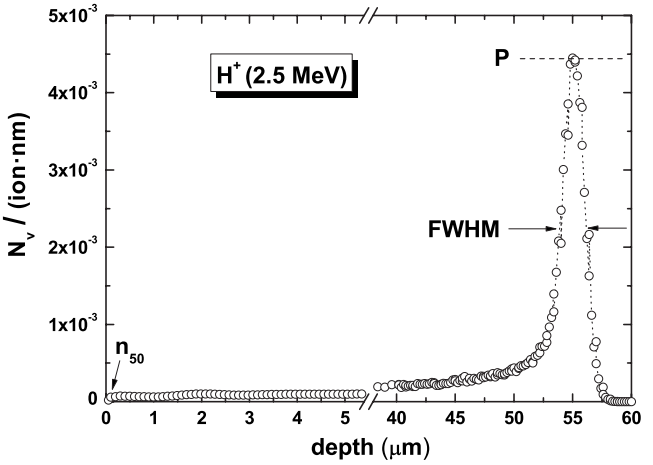

FIG. 1. SRIM calculation of the distribution of vacancies produced in graphite as a function of depth by protons of 2.5 MeV, around the vacancy peak and also close to the surface. The values of vacancy density at 50 nm from the surface, at the peak P and that of its FWHM used in the text are graphically indicated. Contrary to the narrow ion implantation range, there is a rather flat distribution of vacancies produced in the ion track from the surface to the peak region.

In what follows, we estimate that an error of at least 20% should be expected for the calculated damage production rates and the derived mean vacancy distances, arising from three factors: (i) the inherently statistical process of vacancy production, (ii) there is an uncertainty[31] in the necessary energy E_d to produce a vacancy/interstitial pair through ion irradiation in a carbon disordered structure with the graphite mass density (we take $E_d=30\pm7$ eV); and (iii) the used Monte Carlo simulation program does not take into account annealing processes during irradiation and further defect diffusion at the sample temperature of 300 K, temperature at which each sample is kept for one to two weeks after irradiation and before the magnetic characterization.

C. Definitions and procedures for the numerical calculation of vacancies

From the SRIM calculations described above and knowing the used fluences F (expressed in irradiated ions per sample area, i.e., ions/nm^2=10^{14} cm^{-2}), one can determine the rel-

evant total vacancy densities and corresponding mean vacancy distances d_{vac} produced in our irradiation experiments, as we explain below. Note that these vacancy densities (or distance between them) are nominally maximum (minimum) values because of the reasons described above.

In the highest-damaged region within a depth range equal to full width at half maximum (FWHM), see Fig. 1, where most of ions stop, we will consider an average vacancy density $P/2$, P being the peak value of vacancy density. The isotropic average distance between vacancies $d_{vac,peak}$ in this highly defective region will be then given by $1/d^3_{vac,peak} = (P/2)F$. We will also take into account the vacancy density at 50 nm from the surface n_{50} (i.e., its average value in the first 100 nm from the graphite surface, see Fig. 1). In this case, the mean distance between vacancies $d_{vac,50}$ at 50-nm depth will be obtained from $1/d^3_{vac,50} = n_{50}F$. All these values for each irradiated sample are given in Table I.

III. EXPERIMENTAL DETAILS

A. Experimental setup and sample handling

1. Irradiation of the samples

All the irradiation experiments were performed using the 5-MV tandem accelerator of the Center of Micro-Analysis of Materials (CMAM) at the Universidad Autonoma de Madrid.[34] The voltage at the accelerator terminal is regulated by a Cockcroft-Walton-type power supply, with a ripple of less than 50 V for a terminal voltage of 5 MV. The fluence on the sample is measured with the help of a transmission Faraday cup, which monitors continuously the current during irradiation. Two sample holders can be mounted in the irradiation chamber bringing two samples to equivalent positions in front of the ion beam after a rotation of 180°: the sample to be irradiated and a quartz sample used as a reference. Figure 2 shows one of the individual sample holders (left photo) as well as two sample holders mounted in the irradiation chamber as seen through a port (right photo).

The ion luminescence of the quartz sample is used to check the shape and uniformity of the beam over the irradiated area with the help of a high sensitivity charge coupled device (CCD) camera with its control of gain, contrast, and exposure time. Figure 3(a) shows a photo taken by the CCD camera of the quartz sample when irradiated by the beam. In this way, this irradiated area can be defined with a precision of around 20%. As the fluence is determined by the current density on the sample, its precision is directly related to that of the irradiated surface and will be also of ~20%. During irradiation, a thermal image (system Variocam from InfraTec GmbH) is obtained from the sample through a diagonal ZnSe viewing port, monitoring in real time the temperature of the sample surface during irradiation with an accuracy of ± 2 K. Figure 3(b) shows one of these thermal images obtained during the irradiation with 8.5-MeV protons of sample S12. Note that the second sample holder with the reference quartz sample [still warm after its previous irradiation, see Fig. 3(a)] is also observed on the left.

2. SQUID

At magnetic fields $B \leq 1$ T the reproducibility of commercial SQUID's with the reciprocating sample option (RSO) is usually better than 1 μemu and therefore these magnetometers can be used to measure the effects produced by irradiation, see, for example, Ref. 12. Care should be taken, however, with possible artifacts of these systems, specially magnetic field hysteresis due to the electronics and/or to the superconducting solenoid. The reproducibility of each SQUID system should be checked before starting the irradiation steps. We note that the SQUID sensitivity without this RSO option is not enough to measure accurately the effects produced by irradiation, specially when the induced changes in the magnetic moment are ≤ 1 μemu. The magnetic-moment measurements were performed with two SQUID magnetometers from Quantum Design with the RSO. In all the measurements presented in this paper the magnetic field was applied parallel to the graphene planes in order to diminish the contribution of the diamagnetic background.

3. Handling of sample holders

Once the sample has been measured before irradiation, it should be transported to the irradiation chamber and back to the SQUID holder without touching the sample or its holder, avoiding to change their relative position. Special care should also be taken not to introduce additional impurities. Therefore, a minimization of sample handling is absolutely necessary. It is also important to avoid changes in the misalignment between sample position and field, i.e. the angle between magnetic field and sample c axis, inside the SQUID since the diamagnetic background is very sensitive to this angle. To accomplish these requisites, we have designed a sample holder that allows us to measure the magnetic moment of the sample in the SQUID and to fix it inside the irradiation chamber without any changes. A photo of one of the used sample holders is shown in Fig. 2. A further increase in the reproducibility is obtained when the same sample position in the x,y plane inside the SQUID is selected. To do this one rotates the sample on its holder axis till the diamagnetic signal is minimized.

We investigated the reproducibility of the magnetic signals and checked that the sample handling after irradiation of the sample several times with negligible fluences does not produce systematic changes in the magnetic signals. Our arrangement provides a reproducibility better than 2×10^{-7} emu up to 1 T field and allows the subtraction of the virgin data from those after irradiation point by point, increasing substantially the sensitivity of the magnetic measurements. In this way we obtain directly the effect produced by the ion irradiation on the magnetic response of the HOPG samples.

B. Main characteristics of the irradiated samples

All used graphite samples were HOPG from Advanced Ceramics with a rocking curve width of 0.4° (grade A). Using particle-induced x-ray emission (PIXE) we measured the impurity content of the graphite samples. This is (all numbers in μg/g): Ti=2 ± 1, Fe=0.4 ± 0.2, V=8 ± 1, Cr<0.1, Ca<0.02, Ni<0.1, Cu=0.2 ± 0.2, Zn≤ 0.3, and Zr<2. The concentration of magnetic impurities is very small and can be transduced in less than one magnetic atom per 10^6 carbon

TABLE I. Sample data, including irradiation parameters and estimation of induced damage, as follows: sample code; ion used for irradiation; ion energy E; area of irradiation spot A_{spot}; total implanted charge Q_{total}; irradiation time t_{irr}; typical current I; highest surface temperature during irradiation T_{surf}; fluence F; ion range of implantation R; FWHM of the vacancy density distribution; average distance between vacancies at half-maximum of the density distribution $d_{vac,peak}$; average distance between vacancies at 50-nm depth $d_{vac,50}$; and total number of produced vacancies N_v.

Sample	ion	E (MeV)	A_{spot} (mm^2)	Q_{total} (μC)	t_{irr}	I (nA)	T_{surf} (°C)	F (ions/nm^2)	R (μm)	FWHM (μm)	$d_{vac,peak}$ (nm)	$d_{vac,50}$ (nm)	N_v (10^{17})
S1	C^{4+}	25	12.2	53.4	2 h	7.5	100	6.83	19.8	0.40	0.71	3.9	0.54
S2a	C^{4+}	25	12.2	427	12 h	10	140	54.7	19.8	0.40	0.35	1.9	4.3
S2b	C^{4+}	$5\times(2,\ldots,1.2)$	4.1	42.14	1 h 20 min	$11,\ldots,6$	$48,\ldots,35$	$27.6,\ldots,7.6$	$1.90,\ldots,1.35$	0.25	0.38	0.63	1.3
S3	C^{4+}	25	12.2	180	5 h	10	140	23.0	19.8	0.40	0.47	2.6	1.8
S5	C^{4+}	25	12.2	92.3	2 h 40 min	9.5	120	11.8	19.8	0.40	0.59	3.2	0.93
S7	N^{4+}	22.7	12.2	35.6	1 h	10	88	4.56	13.7	0.37	0.71	3.5	4.0
S8	N^{4+}	22.7	12.2	35.6	6 h 30 min	1.5	50	4.56	13.7	0.37	0.71	3.5	4.0
S9	H^+	2	8.4	840	10 h	38	74	624	38.1	1.9	0.82	3.4	1.0
S10	H^+	$5\times(2,\ldots,1.2)$	4.8	3800	14 h 45 min	$60,\ldots,90$	$70,\ldots,100$	$1562,\ldots,624$	$38.1,\ldots,16.7$	$1.9,\ldots,0.9$	0.60	1.6	4.7
S11	H^+	2	4.2	1200	6 h 30 min	45–60	95–115	1783	38.1	1.9	0.58	2.4	1.4
S12	H^+	8.5	16	1200	22 h 30 min	15	105	468	457	19	1.7	6.4	2.8
S13	H^+	4	20	2705	8 h	80–90	51	844	122.5	4.7	1.0	4.0	4.3
S14	H^+	2.5	14	1458	3 h 25 min	120	19	455	55.1	2.4	1.0	4.6	1.3
S15	H^+	5.5	20	4200	16 h 30 min	50–70	90	1307	213	9.5	1.0	3.4	7.8

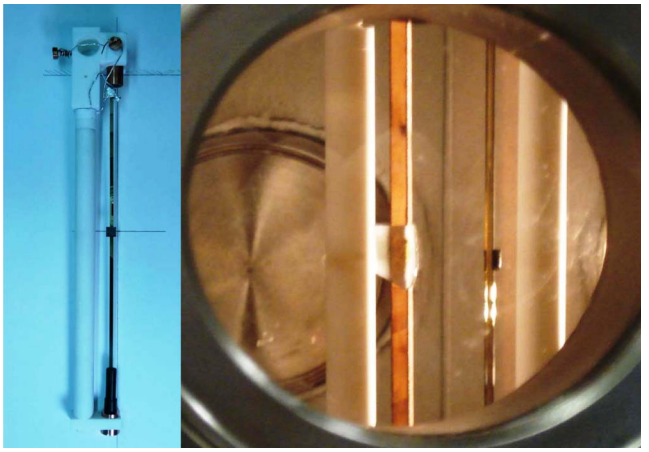

FIG. 2. (Color online) Left photo: sample holder ready for being mounted into the irradiation chamber. Graphite sample is fixed to the specially designed sample holder made of golden quartz for the SQUID, that in turn is attached to a setup made of MACOR designed to fit into the irradiation chamber. Right photo: quartz (foreground) and graphite sample (background) already mounted in the irradiation chamber. A rotary feedthrough allows placing them at the irradiation position from outside of the chamber without breaking vacuum.

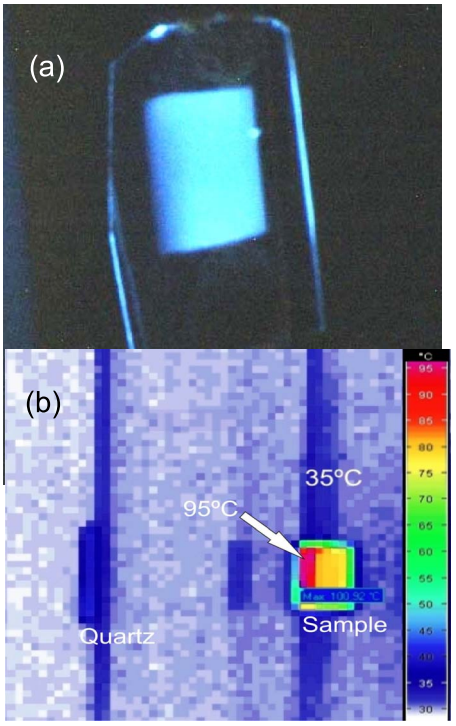

FIG. 3. (Color online) (a) Quartz sample used as reference when irradiated by a proton beam of 8.5 MeV. Light produced due to ion luminescence is used to determine size (4 mm×4 mm in this case) and homogeneity of the ion beam prior to graphite irradiation. (b) Thermal image from the sample S12 obtained with an infrared camera, taken through a diagonal viewing port, monitoring in real time the temperature of the sample surface during irradiation (8.5 MeV protons, in this case). Note the inhomogeneous temperature distribution on the sample surface during irradiation, here typically ranging from 70 °C to 95 °C. The other sample holder with the reference quartz sample [still slightly warm after its previous irradiation shown in (a)] can also be seen on the left.

atoms, a concentration that we can neglect regarding its influence in the magnetic phenomena we observed after irradiation.

The PIXE measurements were done with low fluence of protons of 2.5-MeV energy in order to leave fairly undisturbed the graphite lattice previous to the irradiation needed to produce a certain amount of defects. The 2.5-MeV protons used by PIXE provide an average impurity concentration up to a depth of 57 μm from the sample surface, see Fig. 1. This penetration range covers those of all but three of the studied samples, see ion range in Table I. Furthermore, we note the following; due to the used subtraction procedure, see Sec. IV A, the presented magnetic signals are those triggered only by the irradiation, independently of the amount of impurities, which is not changed. Secondly, recently done XMCD measurements on HOPG bulk samples[18] as well as the results from Ref. 13 indicate that most, if not all, the triggered ferromagnetism by the irradiation is concentrated in the first micrometer near surface region, a region that the PIXE method certainly characterizes.

As shown in detail in Table I, four samples (S1–S5) were irradiated by carbon ions at 25 MeV with different fluences. One of them (S2b) was subjected to a further multiple-energy irradiation (five irradiations between 1.2 and 2 MeV with an energy step of 0.2 MeV) a few months later. Two samples (S7–S8) were irradiated with nitrogen ions at 22.5 MeV (with the same fluence but using different currents).

Seven samples (S9–S15) were irradiated by protons using different fluences, currents, and ion energies ranging from 1.2 to 8.5 MeV. Three of these samples (S13–S15) were taken out of the above-mentioned golden quartz sample holders to be fixed in other oxygen-free high-conductivity (OFHC) copper sample holders that were attached to a cold finger in the irradiation chamber. The reason for this preparation was to decrease the temperature of the sample during irradiation to try to increase the ferromagnetic signal as was observed in Ref. 13. As can be seen in Table I, although this cold finger allowed us either to decrease the sample temperature or to increase the applied current for a given temperature, it was not possible to cool down the sample to ~100 K as in Ref. 13. Nevertheless, we want to stress that these surface temperatures are only indicative since there will be a heterogeneous distribution of temperatures along the sample interior that is difficult to know.

After irradiation the samples S13–S15 were removed carefully from those OFHC substrates and fixed again on the usual SQUID sample holder. Due to different misalignments between sample and field the diamagnetic contribution changed and therefore it is not straightforward the subtraction to obtain the absolute change in the magnetic moment and its temperature dependence. That is why the errors in the obtained parameters for these samples are larger than for the rest of the samples.

IV. DATA TREATMENT AND THEORETICAL DESCRIPTION OF THE TEMPERATURE AND MAGNETIC FIELD DEPENDENCE

A. Field and temperature dependence of the magnetic moment produced by the irradiation

The applied field (H) dependence of the measured magnetic moment shows in general a diamagnetic response of the form

$$m_D(H,T) = \chi_{\mathrm{dia}}(T) m H, \tag{1}$$

where χ_{dia} is the diamagnetic susceptibility and m the sample mass. In our case and because the applied fields are parallel to the graphene layers, this susceptibility should be, in principle, the intrinsic one $\chi_{\mathrm{dia},\parallel}$. It turns out that this $\chi_{\mathrm{dia},\parallel}$ is, in general, much smaller than the measured one, which comes mainly from a small sample misalignment. An applied magnetic field component normal to the graphene planes of the sample induces a negative magnetic moment due to the Landau diamagnetism induced on the graphene layers, what makes the diamagnetic susceptibility of graphite to be so much anisotropic. In our case and for all samples except S13–S15, this misalignment remains constant allowing us to subtract the magnetic moment before irradiation from the data obtained after irradiation. In this case the subtraction we present in this work shows us exclusively the irradiation effects on the sample magnetism. Therefore, it is unnecessary to subtract $m_D(H,T)$ from the measured data as it is usually done in literature to reveal the irradiation effects. Other advantage of this data treatment is that for comparison with theory the real sample mass or volume plays no role, but rather the absolute number of defects the irradiation induces.

The use of the same sample holder for SQUID measurements and the irradiations allows us to calculate the magnetic moment difference defined as

$$m_{diff}(T) = m_a(T) - m_b(T) \tag{2}$$

at fixed temperature T or the difference

$$m_{diff}(H) = m_a(H) - m_b(H) \tag{3}$$

at a fixed applied field, which in our case we will take always equal to 1 T. The subindices a,b in the Eqs. (2) and (3) stand for the moment after and before irradiation, respectively.

B. Paramagnetic response: One and two multiplets cases

The response of free, independent magnetic moments under an applied magnetic field H and without interaction between them gives rise to paramagnetism. As a function of field and temperature the magnetic moment m_P (the magnetization M multiplied by the sample mass or volume) due to this effect follows the Brillouin function $B_J(y)$ where, for independent magnetic lattice ions, J denotes the total angular moment and the variable $y \propto \mu_0 H/k_B T$.

For $y \ll 1$ the susceptibility $\chi = M/H$ follows the Curie law C/T being C the Curie constant. In our case and because we obtain the temperature dependence always at a fixed field of $\mu_0 H = 1$ T we will write for the classical paramagnetic contribution of N paramagnetic centers, each with an effective magnetic moment $\mu_{\mathrm{eff}} = p\mu_B$ (μ_B is the Bohr magneton), as

$$m_P = C/T, \tag{4}$$

$$C = N\frac{\mu_{\mathrm{eff}}^2}{3k_B} = Np^2 \ \ 2.08 \times 10^{-15} \ \ \mu\mathrm{emu\ K}. \tag{5}$$

For the case of atomic paramagnetic centers the effective Bohr magneton number is given by[35] $p = g(JLS)\sqrt{J(J+1)}$ where $g(JLS)$ is the Landé factor. However, for the case of paramagnetic centers due to (multi-) vacancies (or interstitials) neither the value nor the analytical dependence of p on the defect characteristics is known. Our results provide a first experimental value for this number. At low-enough temperatures the paramagnetic response follows a s-like curve with saturation of m_P at high-enough magnetic fields, i.e. at $y \gg 1$.

The usual paramagnetic Curie law assumes that only one multiplet contributes with its $2J+1$ magnetically generated and equally spaced sublevels. However, due to the disorder (including vacancies and the influence hydrogen can have on triggering localized magnetic moments in carbon structures[9,19,36]) more than one multiplet may contribute to the observed paramagnetic response, specially if the energy of the first excited multiplet is not far above the ground-state multiplet. There are only a few examples in the literature for this kind of paramagnetism.[37] An approximate expression for the paramagnetic contribution of two multiplets separated in energy by a magnetic field and temperature-independent gap Δ can be given as

$$m_P = N\frac{\sum_{m^\star=-J}^{J} -x_1\mu_1(m^\star)\exp[-\mu_1(m^\star)\mu_0 H/k_B T] + \sum_{m^\star=-J'}^{J'} -x_2\mu_2(m^\star)\exp\{[-\mu_2(m^\star)\mu_0 H - \Delta]/k_B T\}}{\sum_{m^\star=-J}^{J}\exp[-\mu_1(m^\star)\mu_0 H/k_B T] + \sum_{m^\star=-J'}^{J'}\exp\{[-\mu_2(m^\star)\mu_0 H - \Delta]/k_B T\}},$$

$$\mu_{1,2}(m^\star) = g^\star_{1,2} m^\star \mu_B, \tag{6}$$

where we assume x_2 as the fraction of paramagnetic centers where two multiplets [instead of the single ones, in Eq. (6) with concentration x_1] contribute effectively to the total magnetic moment m_P. In Eq. (6) the magnetic moments $\mu_{1,2}$ are functions of the quantization number $m^\star$ on which the statistical average is done, $g^\star_{1,2}$ are the effective g factors of the corresponding magnetic moments. The other constants are $\mu_0 = 4\pi 10^{-7}$ H/m and $\mu_B = 9.27 \times 10^{-21}$ emu. Because we do not deal with simple atomic multiplets, all the parameters included in Eq. (6) as the $m^\star$ as well as the g factors, should be, in general, taken as effective values till a general theory for the treatment of magnetic moments due to lattice defects including multivacancies is developed.

As we shall see below, the paramagnetic response of one of the irradiated samples suggests the contribution of more than a single ground-state multiplet. To compare with experimental data we assume the simplest case of two different multiplets, the ground state with a twofold zero-field degeneracy $m^\star = -1/2, 1/2$ and a $g^\star_1$ factor and the second, shifted by Δ from the ground state, paramagnetic multiplet with four fold $m^\star = -3/2, \ldots, 3/2$ degeneracy and $g^\star_2$ factor. These simple assumptions describe reasonably well the data. The four parameters we obtain from the fits are then: the two $g^\star_{1,2}$ factors, the energy difference Δ and the total number of paramagnetic centers N. Note that assuming a multiplet of higher order (larger J) decreases the $g^\star$ factor necessary to fit the data. The fits to the data show that Δ is a robust value, which remains independent of the maximum J assumed for the multiplets. The physical meaning of $J, m^\star$ and $g^\star$ of the magnetic moments produced by the lattice defects is certainly not the same as the ones used in the atomic model.

C. Beyond the classical paramagnetic response

The results we have obtained indicate that the ion irradiation not only induce the classical paramagnetism and ferromagneticlike response but also an extra, anomalous magnetic contribution. As we shall see in the next section, this magnetic contribution increases linearly with applied field, as we would expect for a paramagnet when the ratio $\mu_s \mu_0 H / k_B T \ll 1$ (μ_s is the magnetic moment of the paramagnetic centers). However, the measured temperature dependence indicates that this extra contribution remains practically constant below 100 K in contrast to the classical paramagnetic case. The results suggest that in the irradiated samples where no ferromagnetism is obtained, magnetic clusters are induced with anomalous characteristics, probably a kind of precursors to a state where ferromagneticlike correlations starts to be relevant.

Phenomenologically we found that the temperature dependence of the anomalous magnetic contribution $m_A(T)$ follows the dependence given by the implicit equation

$$\frac{m_A(T)}{m_0} = L\left\{3\frac{T^\star}{T}\left[\frac{m_A(T)}{m_0} + h\right]\right\}, \tag{7}$$

where $L(x)$ is the Langevin function given by

$$L(x) = \frac{1}{\tanh(x)} - \frac{1}{x} \tag{8}$$

$T^\star$ is a critical temperature above which this contribution vanishes, the parameter $h < 1$ determines the slope in temperature of the curve around $T^\star$, and the magnetic moment $m_0 = m_A(T=0)$. Equation (7) resembles the equation one uses within the Weiss model in the classical limit for the temperature dependence of the magnetization *at constant magnetic field* of a ferromagnet. As we will discuss below the measured field dependence of this anomalous paramagnetism is not given by the Weiss model but it shows a linear field dependence in the whole temperature range.

D. Quasi-two-dimensional magnetic order

In a previous work it has been demonstrated that the temperature dependence of the ferromagnetic magnetic moment induced in graphite by proton irradiation decreases unequivocally linearly with temperature.[13] This linear dependence has been taken as an indication for two-dimensional (2D) magnetism (with anisotropy). The temperature slope can be interpreted as due to the excitation of 2D spin waves that reduce the magnetic moment linearly with T. For more details on these theoretical aspects and the comparison between experiment and three-dimensional and 2D theories, we refer to Refs. 13 and 38–40. For simplicity we will fit the ferromagnetism induced by irradiation in graphite using the following linear relation:

$$m_{\mathrm{FM}} = m_0 - aT, \tag{9}$$

where a is a free parameter related to the renormalized exchange interaction of the low-energy spin excitations.[13]

V. EXPERIMENTAL RESULTS

Because of the lack of knowledge of the amount of sample that is magnetic after irradiation, all the SQUID data are the directly measured magnetic moments. Although one knows the penetration depth of the ions for the used energy in graphite, the sample ranges where the main ferromagnetic and paramagnetic signals come from, are not necessarily the same.[16] Therefore, it has little sense to divide the values of magnetic-moment differences m_{diff} by the total sample mass. Taking into account recently done XMCD and magnetic force microscopy measurements of irradiated spots in 200-nm carbon films[17] it is expected that the ferromagnetic layer in our samples is mainly located at the first micrometer from the sample surface. This assumption has obtained further support from recently done XMCD studies on HOPG surfaces.[18]

A. Paramagnetism induced by ion irradiation

Figure 4(a) shows the field dependence of the magnetic moment produced by the irradiation m_{diff} at three temperatures for sample S1 after irradiation with C^+ ions, see Table I. The obtained changes show a clear linear dependence with field up to room temperature with no sign of any nonlinear behavior with magnetic field. This means that this irradiation

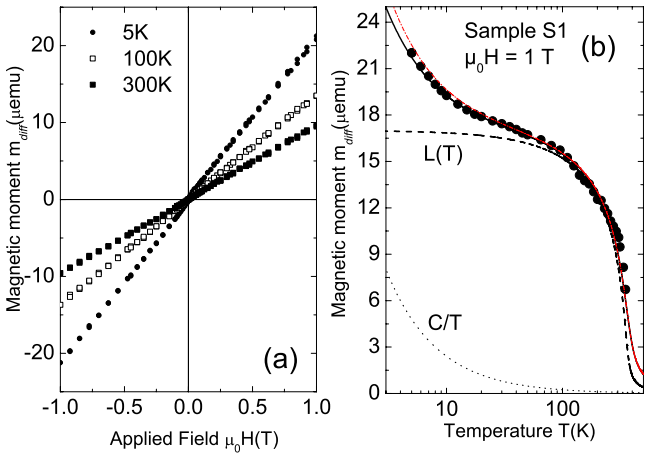

FIG. 4. (Color online) (a) Difference in magnetic moment $m_{diff}(H)$ as a function of field at three different fixed temperatures. Note the absence of any nonlinear behavior. (b) The same but as a function of temperature at a fixed field of 1 T. The dotted curve follows the paramagnetic Curie-law C/T with $C=25$ μemu K. The dashed curve follows the Langevin function [Eq. (7)] with $h=0.01$, $m_0=17$ μemu and $T^\star=350$ K. The continuous line is the sum of the Curie contribution and that given by Eq. (7) with $h=0.03$, instead of 0.01. The dashed dotted (red) line was obtained with similar parameters but with C 15% larger. The difference between the two fits is at low temperatures larger than the error bar of the data, which is ± 0.2 μemu.

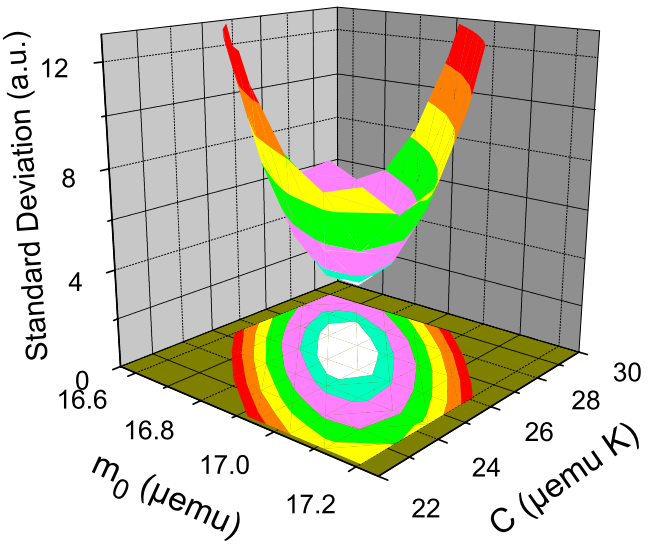

FIG. 5. (Color online) Standard deviation between the fits and the experimental data from sample S1 shown in Fig. 4(b) as a function of the two free parameters used, namely, C from Eq. (4) and m_0 from Eq. (7). The other parameter h does influence only the fit near $T^\star$ and it is not shown in this correlation matrix for clarity.

neither did induce ferromagnetism in the sample nor decrease its intrinsic ferromagnetism, within experimental error. A similar behavior has been found for samples S2, S5, S13, S14, and S15. As examples, we will present here the results of some of those samples.

Although the behavior appears compatible with a pure paramagnetic one, there is no H/T scaling, a fact that is recognized due to the relative small decrease in m_{diff} with increasing temperature and at all fields. This behavior does not match with the classical Curie-law paramagnetism as the temperature dependence of the magnetic-moment difference clearly shows at an applied field of 1 T, see Fig. 4(b). The continuous line in Fig. 4(b) has been obtained as the sum of a Curie-type dependence [see Eq. (4)] plus an extra "anomalous" contribution given by Eq. (7) with the parameters $h=0.03$, $m_0=17$ μemu and $T^\star=350$ K.

Figure 5 shows the correlation of the standard deviation between the fits and the data of sample S1 [Fig. 4(a)] and the two free parameters used, i.e. C and m_0. The minimum deviation is achieved at $C \simeq 26 \pm 1$ μemu K and $m_0 \simeq 16.9 \pm 0.2$ μemu. In general, the correlation between these two parameters as well as between C and the ferromagnetic linear terms [Eq. (9)] provides an error in the determination of C of less than 15%. This error as well as errors from other sources were taken into account in the discussion, see Figs. 13 and 14.

We note that for all irradiated samples in which the irradiation *did not* induce a ferromagnetic contribution, $m_{diff}(T)$ at a fixed field can be very well fitted adding the Curie-type Eq. (4) and the anomalous contributions $m_A(T)$ from Eq. (7). A further example is shown in Fig. 6(a) where we present $m_{diff}(T)$ for sample S2 after the first (S2a) and second (S2b) irradiation. The continuous lines in Fig. 6(a) were obtained with the same equations as in Fig. 4(b) but with different parameters. Whereas the Curie constant C is ~3 larger in S2

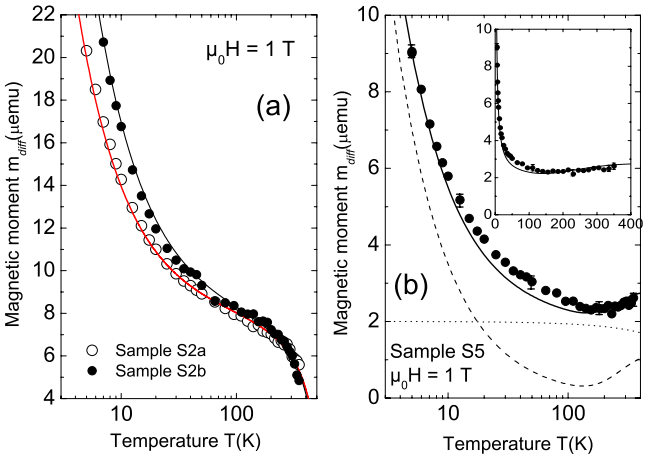

FIG. 6. (Color online) (a) The difference in magnetic moment $m_{diff}(T)$ at 1 T for samples S2a and S2b. The continuous lines were calculated using Eq. (7) as in Fig. 4 and with the parameters $C=60(90)$ μemu K, $m_0=8$ μemu, $h=0.01$, and $T^\star=490(473)$ K for the sample S2a (S2b). (b) The same as in (a) but for sample S5. The dashed line was calculated following Eq. (6) with the parameters $\Delta=850$ K, $g_1^\star=1$, $g_2^\star=10$, the weights $x_1=0.9$ and $x_2=0.1$ for the first and second contributions and $N\mu_B=2.3\times10^{-4}$ emu. The dotted line follows Eq. (7) with $m_0=2$ μemu with a $T^\star=1000$ K. The small deviation between the simple model used and the data can be easily diminished by taking a distribution of the parameter Δ instead of a fixed one. This has sense physically since the magnetic defects that contribute to the excited multiplet, such as multivacancies, are not all exactly the same in the irradiated matrix. The inset shows the same data but on a linear temperature scale.

than in S1, the anomalous contribution given by m_0 is nearly two times smaller suggesting a possible balance between these contributions and the amount of induced defects. We note, however, that taking into account all the parameters obtained from the $m_{diff}(T)$ fits of all samples we could not find any obvious correlation between these two contributions. For example, sample S5 shows $C=30$ μemu K and $m_0=2$ μemu but for sample S13 we obtain $C=45\pm15$ μemu K and $m_0=2.7$ μemu. A relationship between the Curie constant C and the nominally induced vacancy density is found and will be discussed in Sec. VI as well as the possible origins of the anomalous contribution.

As discussed in Sec. IV B, a pure Curie-type paramagnetic contribution applies only for a single ground-state multiplet with $2J+1$ equally spaced levels and $y \ll 1$. In case there is a second multiplet no so far away in energy from the first ground state one, then we may expect an anomalous behavior at high-enough temperatures, when the lowest energy states of the second multiple starts to be occupied. The results obtained for sample S5 suggest such a contribution, see the slight increase in m_{diff} at T 100 K in Fig. 6(b), which is in clear contrast with the dependence expected from the usual Curie or Langevin laws. From the fit we obtain that $\sim$10% of the paramagnetic centers have a second multiplet shifted $\sim$850 K in energy from the ground state level, see Fig. 6(b). Since statistically speaking ion irradiation may create regions with clusters of a different defect density or even types of lattice defects in the graphite structure, the observed behavior in sample S5 could be, in principle, expected. We stress that the $g_i^\star$ values obtained from the fits should be taken as effective ones since their meaning is still open; note that not an atom but several atoms around a single or multivacancy originate the magnetic moment. Surprising is actually that ion irradiation in the MeV energy creates mostly defects with a multiplet well below in energy from the first excited one. A systematic and well-reproducible paramagnetic contribution with two multiplets shifted by $\Delta \sim 200-900$ K in energy has been recently found in annealed Kapton,[41] an aromatic polymer that graphitizes when heated at very high temperatures.[42]

B. Ferromagnetism induced by ion irradiation

Ferromagnetism has been induced by ion irradiation in the HOPG samples S3, S8, S10, and S11, where the last two samples were irradiated with similar parameters as in previous work.[11,13] Figure 7(a) shows the magnetic-moment difference as a function of applied field for sample S10 at three different temperatures. The *s*-like behavior at low fields is clearly recognized in that figure suggesting the existence of magnetic order with a Curie temperature above room temperature. The temperature dependence of the induced magnetic change is shown in Fig. 7(b). Figure 8 shows the results from the SQUID measurements for the magnetic moment before and after irradiation.

The magnetic-moment difference $m_{diff}(T)$ in Fig. 7(b) appears to be similar to that shown in Figs. 4(b) and 6(a). However, apart from the Curie-type contribution given by Eq. (4) the observed temperature dependence indicates the existence of an extra contribution, which decreases linearly with temperature, in contrast to the anomalous one. The obtained linear contribution in $m_{diff}(T)$ follows Eq. (9) and indicates the existence of a quasi-2D magnetic order in agreement with the existence of the nonlinear *s*-like hysteresis loops at low fields ($\mu_0 H < 0.3$ T) and high temperatures. The linear T contribution can be better visualize in a linear scale, as shown in Fig. 9(b). The observed behavior agrees with the existence of *s*-like hysteresis loops, as shown in Fig. 9(a) for sample S11.

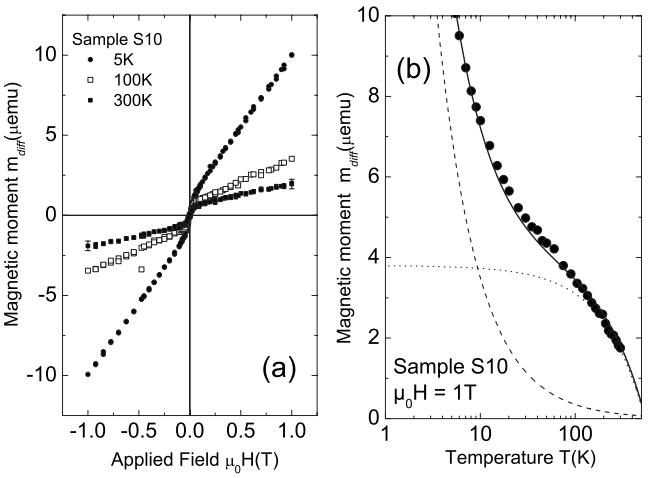

FIG. 7. (a) Field dependence of the difference in magnetic moment $m_{diff}(H)$ at three fixed temperatures for sample S10. Note the clear nonlinear behavior at low fields indicating the existence of ferromagnetic behavior induced by proton irradiation. (b) The difference in magnetic moment $m_{diff}(T)$ at 1 T for sample S10. The dashed line follows the Curie law with $C=35$ μemu K and the dotted line the approximation for the magnetic order in the quasi-two-dimensional case of Eq. (9) with the parameters $m_{FM}=(3.8-7\times10^{-3}$ T) μemu (with T in K). The continuous line is the sum of these two contributions.

Within experimental resolution it is not possible to rule out the contribution of the anomalous paramagnetic contribution in these samples. In fact the positive slope of $m_{diff}(\mu_0 H > 0.1$ T) at 300 K, see Fig. 7(a), suggests that the

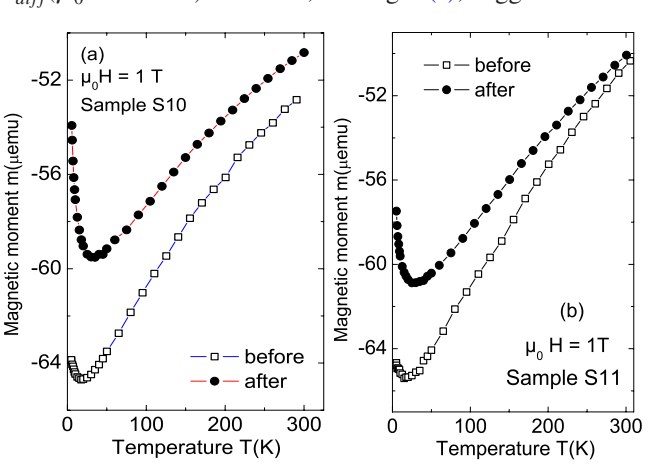

FIG. 8. (Color online) Magnetic moment before and after irradiation (at 1 T field) without any subtraction for sample S10(a) and sample S11 (b).

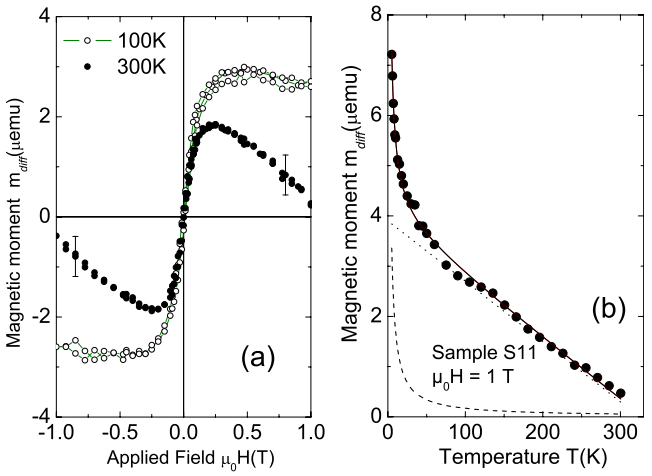

FIG. 9. (Color online) (a) Field dependence of the difference in magnetic moment $m_{diff}(H)$ at two fixed temperatures for sample S11. (b) The difference in magnetic moment $m_{diff}(T)$ at 1 T for sample S11. The continuous line is the sum of these two contributions, namely, the Curie law with $C=17$ μemu (dashed line) and the approximation for the magnetic order in the quasi-two-dimensional magnetic order with the parameters $(3.9-12)\times10^{-3}$ T) μemu (with T in K) (dotted line). The inset shows the measured magnetic moment before and after irradiation (at 1 T field) without any subtraction.

induced anomalous contribution is not zero. The field and temperature dependence of m_{diff} indicates that at 1 T applied field this anomalous contribution should be $\lesssim 1$ μemu.

C. Influence of self-heating during irradiation

As noted in the introduction, one of the disadvantages of ion irradiation to induce magnetic order in graphite is the sample heating during the irradiation. As measured with our infrared thermographic camera, the surface temperature of the samples during irradiation shows a relevant increase, see Table I. The real temperature increase, however, in some parts of the sample interior is certainly higher as the one shown by the measurement. It is known that annealing at low and moderate temperatures diminishes the defect-induced magnetism in graphite.[15,43] For example, Ref. 15 reported the complete vanishing of the C^+-induced magnetic order after annealing the graphite sample at 473 K or at 773 K for 1 h. It is interesting to note that annealing the virgin samples diminishes the ferromagnetism and paramagnetism of graphite, supporting their defect-induced origin.

We would like here to provide further evidence supporting the detrimental effect of annealing on the defect-induced magnetic order presenting the results of one of the virgin HOPG samples before irradiation. This sample showed a rather large ferromagnetic response, see Fig. 10. After annealing it 12 h at 700 K inside the SQUID, without taking it out from SQUID, we observe a clear decrease in both the saturation magnetic moment as well as in the hysteresis width. It is therefore expected that an increase in temperature during irradiation should have a negative effect in the total ferromagnetic mass produced by the irradiation. One expects

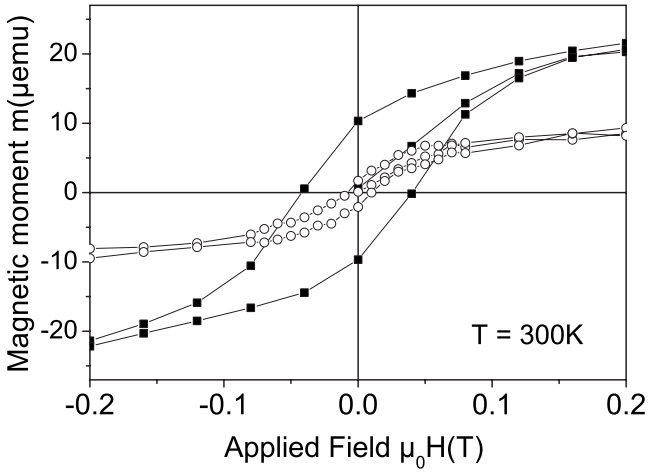

FIG. 10. Room-temperature magnetic moment vs field applied parallel to the graphene planes for a virgin HOPG sample from the same batch as those used for irradiation (■). (○): the same sample after annealing 12 h at 700 K. The hysteresis measurements as well as the annealing were done in the SQUID without taking the sample out of it.

that annealing effects influence the paramagnetic as well. In this section we show the results of samples S7, S8, and S12 as examples for the annealing effects produced by the irradiation.

Figure 11 shows the field dependence of the magnetic-moment difference at three temperatures for sample S8. At 300 K $m_{diff}(H)$ increases slightly with field up to $\mu_0 H$

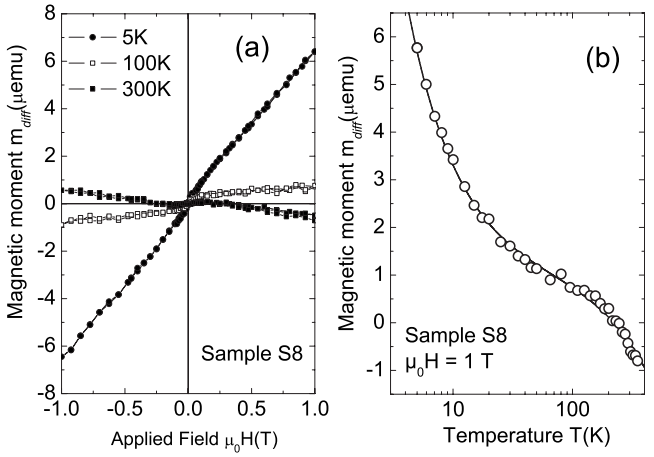

FIG. 11. (a) Field dependence of the difference in magnetic moment $m_{diff}(H)$ at three fixed temperatures for sample S8. Note that the s-like form of the curve at 300 K due to the induced ferromagnetic contribution is nearly parallel to the x axis because of the counter balance coming from a decrease in the paramagnetic response. (b) The difference in magnetic moment $m_{diff}(T)$ at 1 T for sample S8. The continuous line is the sum of two contributions, namely, the Curie law with $C=23.6$ μemu K and the approximation for the magnetic order in the quasi-two-dimensional case, which follows $(1-5\times10^{-9}$ T) μemu (with T in K). Note that above 200 K the difference is negative indicating a decrease mainly in the anomalous paramagnetic contribution due to the annealing during irradiation.

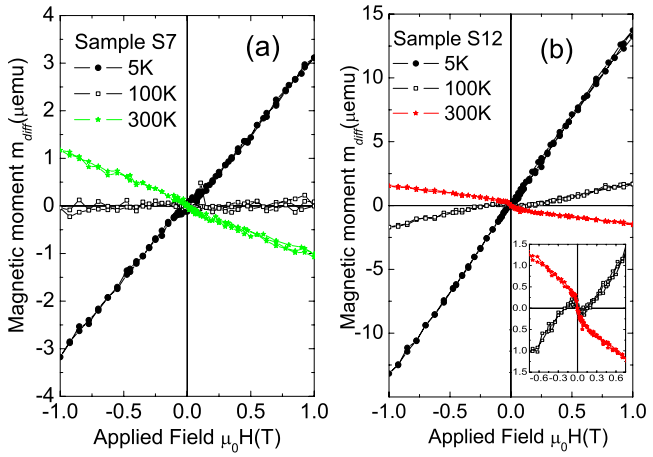

FIG. 12. (Color online) (a) Field dependence of the difference in magnetic moment $m_{diff}(H)$ at 1 T and at three fixed temperatures for sample S7. Note that the inverse *s*-like form of the curve at 300 K due to the decrease in the ferromagnetic contribution. (b) The same difference in magnetic moment for sample S12. The inset shows the data between −0.75 and 0.75 T and for 100 and 300 K.

$\simeq 0.2$ T and decreases at higher fields, see Fig. 11(a). The observed behavior suggests that the irradiation affected mainly the paramagnetic, anomalous contribution part at 300 K (note that at this temperature the usual Curie contribution is negligible). The lower-temperature field data as well as the temperature dependence of m_{diff} at constant field show that the irradiation induced an increase in the Curie-type and ferromagnetic contributions, see Figs. 11(a) and 11(b).

The results of samples S7 and S12 are intermediate cases, which indicate that ion irradiation can induce a broad spectrum of magnetic changes in the graphite structure upon the thermal and ion irradiation conditions. After irradiation the field dependence of m_{diff} for sample S7 indicates a clear decrease in the paramagnetic contribution above ~100 K, see Fig. 12(a). Within experimental resolution $m_{diff}(H)$ is practically linear in field at 5 and 100 K; at this last temperature the difference actually vanishes in the whole field measured range suggesting that no relevant changes in the ferromagnetic or paramagnetic contributions have been induced. At 300 K the weakly noticeable inverse *s*-like form of the curve suggests the decrease in the ferromagnetic contribution. We note that a defect-induced ferromagnetic contribution always exists in the as-received HOPG samples, as shown in Refs. 15, 18, and 44, see also Fig. 10. The irradiation of sample S12 induces more clearly a decrease in the ferromagnetic contribution that we can recognize in the inverted *s* loop at low fields in $m_{diff}(H)$, see Fig. 12(b).

Taking all the results into account we note that the measured surface temperature is not always correlated straightforwardly with the measured increase or decrease of a certain magnetic contribution after irradiation. This nonsimple correlation applies specially when other irradiation parameters such as the ion energy *E*, for example, are also changed (compare the results of samples S11 and S12).

VI. DISCUSSION

The obtained experimental data provide some correlation hints between the observed paramagnetism, the anomalous paramagnetic contribution, and the ferromagnetism induced by the ion irradiation and the produced defects. For clarity we divide the discussion in three parts taking into account the magnetic phenomenon we want to discuss.

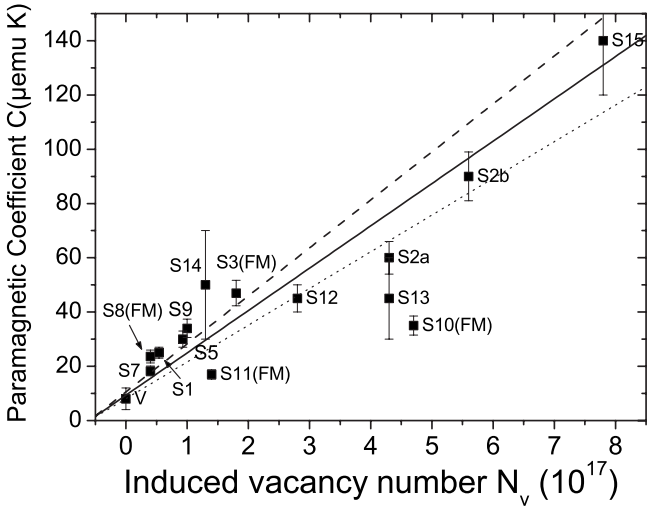

FIG. 13. Paramagnetic parameter *C*, see Eq. (4), obtained from the fits to the magnetic moment difference data as a function of the nominal vacancy number produced by the irradiation for all measured samples. The labels show the sample number and the label "FM" in brackets means that sample shows induced ferromagnetism by the irradiation. The point with the label "V" refers to the samples in virgin, nonirradiated state, with similar volumes. The points from the samples S13–S15 have a larger error in the *C* values because of the different misalignment in the SQUID holder since the samples were taken out of the holders for the lower temperature irradiation. The continuous line is the function $C=0.075\times 2.08\times 10^{-15}(N_V+6\times 10^{16})$. The dashed and dotted lines follow the same function but with the first numerical coefficient equal to 0.085 and 0.065, respectively.

A. Curie-type paramagnetism

This induced paramagnetic contribution is clearly observed at $T<100$ K in all samples. As examples we presented in Figs. 4 and 6 the data for samples S1, S2, and S5. Assuming the usual model for a single, energetically equally spaced multiplet and for $y \ll 1$, the fits to the data using Eq. (4) provide the paramagnetic coefficient or Curie constant *C*, see Eq. (5). Figure 13 shows the obtained *C* parameter as a function of the nominal total number of vacancies N_V produced by the used irradiation for all measured samples. Note that we take only the estimated vacancy number and not the interstitial one. The reason is that whereas the vacancy in the graphite lattice is well defined and expected to have a magnetic moment, the position distribution of interstitials and their effective magnetic moment are not actually known. Also we have taken only single C vacancies because at the ion energies of MeV it is expected that these are those with the highest probability in comparison with multivacancy defects. These multivacancy defects are however produced at low-energy irradiation and may play an important role in the induced effects.[15] We would like also to mention the mea-

surements of ESR linewidths and signal intensity as a function of temperature of graphite samples irradiated with protons, deuterons, and helium,[45] which indicate that the spins produced by the radiation are of a localized nature.

Roughly speaking and within the data dispersion (whose origins we discuss below) we can take a linear correlation between C and N_V given by the equation $C=(0.075\pm0.01)2.08\times10^{-15}(N_V+6\times10^{16})$ μemu K. In this case the effective magneton number for a vacancy would be given by $p=0.27\pm0.02\mu_B$ according to Eq. (5). We can compare this number with the simplest atomic multiplet case. For example, using $p=g(JLS)\sqrt{J(J+1)}$ with $J=S=1/2$, $L=0$, $g=2$ then $p=1.73$. One may speculate that a vacancy itself has no spin, then $S=0$ and $J=L=1/2$, then $p=0.87$. On the other hand, from theoretical estimates[4–6,8,9,36,46] one expects $p\sim0.5,\ldots,1$. Assuming that each vacancy would have an effective magnetic moment of $0.5\mu_B$ the experimentally obtained p is a factor two smaller than expected.

There are several reasons for the smaller value of the effective magneton number p. Firstly, the calculated total number of vacancies N_V is a nominal number obtained using SRIM without taking into account annealing effects, as discussed in Sec. II B. Because without doubt there are annealing effects during irradiation and also after leaving the sample at room temperature[47–49] due to vacancy aggregation and vacancy-interstitial recombination processes the real total vacancy number should be smaller than the one calculated and used in Fig. 13. We must also take into account that part of the vacancies will take part in the induced ferromagnetism as well as in the anomalous paramagnetic contribution. Note that the C values of the samples with the largest induced ferromagnetic moments (S10 and S11) are clearly below the average line, see Fig. 13. In this case it should be clear that the real vacancy number N_V contributing to the Curie-type contribution has to be smaller and in this case the slope of the linear correlation between C and N_V increases as well as the effective magneton number p. Assuming a factor of two smaller number of vacancies than the total one obtained from SRIM that contribute to the Curie-type paramagnetism, the effective magneton number would be then $p\simeq0.5\pm0.2\mu_B$.

The results shown in Fig. 13 as well as the general paramagnetic behavior that virgin bulk HOPG samples below $\sim$50 K exhibit (as examples see Fig. 8), indicate that the paramagnetism in nonirradiated virgin HOPG samples is not necessarily due to impurities but might be also due to lattice defects. From Fig. 13 we would conclude therefore that virgin HOPG samples with 0.4° rocking curve width and a sample volume on the order of 5×10^{-3} cm^{-3} have a vacancy/defect number on the order of 5×10^{16}, i.e., a vacancy/defect density $n_V\sim10^{19}$ cm^{-3}.

This vacancy/defect density is very probably the origin for the carrier density measured in good quality HOPG samples. It has been recently postulated that a relevant part of the measured carrier density (electrons and holes) in graphite is not intrinsic but due to lattice defects and/or impurities.[49] Our results obtained from magnetic measurements agree with this postulate as we show below. The obtained value $n_V\sim10^{19}$ cm^{-3} for the vacancy/defect density in virgin bulk HOPG samples can be translated to a density per graphene layer of $n_V\sim3\times10^{11}$ cm^{-2}. If we assume that each vacancy/defect provides on the order of one carrier to the conduction band,[49,50] then virgin HOPG samples of similar quality would have a carrier concentration at low temperatures of $n_0\sim10^{11}$ carriers per cm^2, in agreement with measured values.[3,51] This evidence plus the studies done in Ref. 49 clearly indicate that the carrier density of graphite samples published in literature is not intrinsic, casting strong doubts on the reliability of tight-binding parameters obtained in the past.

It is also worth mentioning several works[52–54] where point defects at graphite surfaces were generated by low-energy ($\sim$0.1 keV) argon ion sputtering under ultrahigh vacuum conditions, and investigated by scanning tunneling microscopy (STM) and spectroscopy. On ion-bombarded surfaces with atomic vacancies, a large increase in the charge density of states near the Fermi energy level was found.[52,53] This charge enhancement was extended over tens of the surrounding carbon atoms for multiatom vacancy. Note also the STM studies in the vicinity of defects produced by chemisorbed hydrogen on the basal plane of graphite showing a long-range ($\sim$6 nm) modification of the electronic structure.[55] In a very recent work[54] similar STM experiments, complemented by tight-binding calculations, revealed the presence of a sharp electronic resonance at the Fermi energy around each single vacancy on the graphite surface, which was associated with the formation of local magnetic moments. Although limited to the very surface of graphite due to the low ion-energies employed, these experiments support our view of paramagnetism in graphite being originated by magnetic moments localized around vacancy defects.

B. Anomalous paramagnetic contribution

An anomalous paramagnetic contribution can be clearly observed mostly for samples where the irradiation induced no ferromagnetism. We call this paramagnetic contribution anomalous because it remains independent of temperature up to $\sim$100 K whereas there is no saturation or any nonlinearity in the field dependence. This means that this paramagnetism does not follow the usual H/T scaling, i.e. the temperature-independent contribution remains also for applied fields lower than 1 T.

Note that the anomalous contribution cannot be interpreted as due to the contribution of high-order multiplets, as one may suggest comparing Figs. 6(a) and 6(b). The reason is that higher energy multiplets, see Eq. (6), do not provide a temperature-independent contribution below $\sim$100 K, in contrast to the experimental results.

Phenomenologically, we found that this contribution follows very well a temperature dependence similar to that one obtains from the classical molecular field Weiss model for magnetic order using the Langevin function, see Eq. (7). The important difference with the classical model is the observed linear dependence in applied field in all the measured temperature range, actually the fingerprint for the classical paramagnetic behavior. Strikingly, if we compare with the molecular field model the values obtained for the parameter $h\sim0.01,\ldots,0.03$ appear to indicate large magnetic moment clusters. For example, according to this model the parameter

h is basically the ratio between Zeeman and thermal energies at a critical temperature T_c given by

$$h = \frac{\mu_0 H \mu_s}{3 k_B T_c}, \tag{10}$$

where μ_s is the magnetic moment of each paramagnetic center at saturation. Using the data at 1 T and replacing $T_c = T^\star$ we obtain that $\mu_s \sim 15-70 \mu_B$.

Comparing the observed behavior with the different magnetic responses expected from localized magnetic moments, i.e. from paramagnetism to supermagnetism, which includes superparamagnetism, superspin glass to superferromagnetism (for a review see Ref. 56), we note that this anomalous paramagnetic response appears to be a kind of superferromagnetism. In this case ferromagneticlike correlations arise in certain regions or clusters between the localized magnetic moments produced by the irradiation. The interaction between these magnetic moments within a cluster, however, is not robust enough to create ferromagnetic domains. From the linear field dependence we speculate that the size or number of these clusters appears to increase proportional to the applied field. On the other hand the thermal energies at temperatures below $T^\star$ is not enough to suppress the magnetic correlation and hence it does not follow the classical ratio H/T.

Our results on the anomalous paramagnetic response suggest that this contribution is probably due to magnetic clusters, which can be considered as precursors of the ferromagnetic state in the graphite structure. As noted above, see Sec. V B, samples where a ferromagnetic response was induced by irradiation show a much smaller contribution of this anomalous paramagnetism. It is also clear that this anomalous paramagnetic response should exist also in virgin HOPG samples, as the Curie-type paramagnetism and ferromagnetic ones.

C. Ferromagnetism induced by ion irradiation

There is now strong evidence that the origin of the intrinsic as well as the ion-irradiation-induced magnetic order in graphite is related to lattice defects such as vacancies and/or adatoms as hydrogen. The last XMCD measurements on HOPG surfaces before and after irradiation confirm the intrinsic origin of the ferromagnetic signals in as-received HOPG samples[44] and provide evidence that also hydrogen plays a role.[18] From the 14 samples reported in this study only four of them showed an increase in the ferromagnetic signal (S3, S8, S10, and S11). Therefore, it becomes evident that there is a rather narrow window of values for several irradiation parameters, such as fluence, energy, or ion current, necessary to trigger a measurable ferromagnetic signal. It is clear that the selected ion fluence will play a main role because this is one of the parameters that determines the defect density as a function of the penetration depth. Taking into account theoretical models, e.g., Refs. 7 and 9, a small enough distance of the order of 2 nm between vacancies that belong to the same graphene sublattice would trigger a ferromagnetic order with a Curie temperature above 300 K and the signal would be sufficiently large to be measurable with

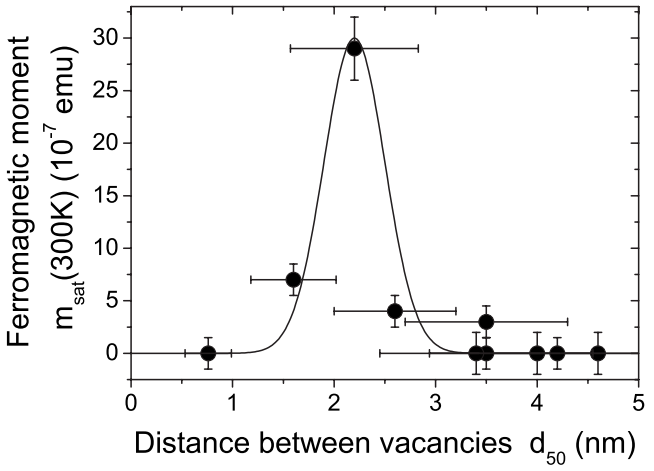

FIG. 14. Ferromagnetic moment at saturation as a function of the nominal distance between induced vacancies calculated at 50 nm from the HOPG surface for most of the samples prepared in this work. The errors bars are the maximum estimated ones considering the sensitivity and reproducibility of the SQUID measurements as well as the range of parameters needed to estimate through SRIM the average vacancy distance within a graphene layer at 50 nm from the sample surface. The continuous line follows a Gaussian function and should be taken only as a guide to the eye.

the SQUID. It should be also clear that the condition of preserving the graphite lattice—amorphous carbon is not ferromagnetic but paramagnetic[57]—provides also a limit to the maximum allowed fluence.

In Ref. 16 the mean distance between vacancies as a function of depth for different proton fluences has been calculated following SRIM estimates. These estimates indicate that the largest ferromagnetic mass one can produce with a single energy proton beam will be located at the first ~ 10-μm depth where this kind of curve is rather flat. Results obtained in Ref. 13 indicate that the measured magnetic signal coming from irradiated spots is located in the first micrometers depth in qualitative agreement with the estimates presented.

In our study we have selected several irradiations where one would expect a rather large part of the sample with a homogeneous concentration of vacancies with distances on the order of 2 nm. However, as demonstrated in the last section, several of those samples, such as, e.g., S7, S8, and S12, did show either a decrease in the ferromagnetic contribution and/or a decrease in the anomalous paramagnetic one, whereas the Curie-type paramagnetic contribution observed at $T < 100$ K always increased after irradiation. The decrease in the ferromagnetic signal after irradiation, see Sec. V C, indicates that self heating effects should be taken into account. It is therefore very probable that this is one of the reasons for the rather small yield of ferromagnetic enhancement after irradiation, remaining one of the main disadvantages this preparation method has, especially if one uses high energy ions.

There is one important point that was not taken into account in the above discussion and it is the influence of hydrogen. If hydrogen plays a role in the enhancement of magnetic order through ion irradiation then it should be clear that this would be triggered in regions where either hydrogen

atoms or molecules already exist or are implanted through the irradiation. The interplay of hydrogen and defects in the enhancement of the magnetic moment at the defect position[36] or just bonded to a carbon atom of the graphene layer[19] has been taken into account in theoretical work in the past. The direct evidence of the influence of hydrogen in the magnetism of graphite through XMCD results[18] indicates that we have to take its role explicitly as a probable trigger for magnetic order by ion irradiation at high energies.

We assume that a similar situation regarding the mean vacancy distance is necessary to trigger a measurable magnetic order, e.g., a mean distance between vacancies on the order of 2 nm but with the presence of hydrogen. From previous[25] and new[26] experimental evidence, we know that the largest amount of hydrogen is found at the surface down to the first micrometer. On the other hand, XMCD measurements indicate that the magnetic order signal after 2-MeV proton irradiation is mainly localized in the first 20 nm from the surface.[18]

Using SRIM, we have calculated the mean distance between vacancies at 50 nm from the HOPG surface (at the used energies the result is independent of whether it is at the surface or 100-nm depth), see Table I. Figure 14 shows the measured ferromagnetic saturation moment at 300 K as a function of the vacancy distance at 50-nm depth from the sample irradiated surface. From this figure it should be clear that the window for triggering a measurable enhancement of the ferromagnetism in HOPG sample using high-energy ions is rather narrow. The results suggest also that at vacancy distances larger than ~ 3 nm no measurable magnetic ordering appears. At vacancy distances smaller than 1.5 nm the structure is probably too disordered that no magnetic order can be triggered. Without taking into account self-heating effects the results shown in Fig. 14 suggest that the magnetic order is triggered in the near surface region when the mean vacancy distance produced by the high-energy irradiation is nominally on the order of 2 nm.

It is important to note that the absolute magnetic moment induced by the ion irradiation is small. But this does not mean that the magnetic order is weak since we have to take into account how large is the total induced ferromagnetic mass. Taking into account the results from Ref. 18 we may take a magnetic thickness $\lesssim 20$ nm. This means that the observed maximum peak in the magnetic moment represents a magnetization of $M \gtrsim 4.7$ emu/g in the irradiated region of the sample S11, a value similar to those reported in Refs. 13–15.

Finally we would like to note that the obtained results in this work have some similarity with the phase diagram suggested by ESR measurements.[24] In particular, the weakly temperature-dependent metalliclike L1D line might be correlated to the anomalous paramagnetic contribution observed here. These regions may grow with irradiation fluence as precursors of the ferromagnetic ones. Of interest is also the correlation of the irradiation triggered ferromagnetic signal with the L1G line observed in Ref. 24. Future studies should use both characterization methods on the same samples and as a function of fluence to clarify the origin of this apparent correlation.

VII. CONCLUSION

In conclusion, the main results of our study are: (a) ferromagnetic states can be induced independently of the ion used, in agreement with published results in literature. However, the results presented in this study indicate that there is a rather narrow window of parameters where this effect can be triggered using MeV ions. Apart from heating effects during irradiation this narrow window is probably related to the mean vacancy distance and the high hydrogen concentration at the near surface region. For samples where this ferromagnetic state was enhanced, a linear temperature dependence of the ferromagnetic moment is found in agreement with ferromagnetic excitations in a quasi-2D lattice. (b) Heating effects during irradiation appear to be important and can induce a decrease in the paramagnetic as well as ferromagnetic initial states of the samples. Self-heating, the further relaxation of defects and hydrogen diffusion at room temperature are some of the reasons for the small yield of ferromagnetic mass using ion irradiation at MeV energies. (c) The Curie-type paramagnetic contribution increases proportional to the nominal-induced vacancy number with an effective Bohr magneton number $p = 0.27 \pm 0.02 \mu_B$. Taking into account the vacancy aggregation and vacancy-interstitial recombination processes, even at room temperature,[49] this value should be taken as a lower limit. (d) We found a new intermediate magnetic state in samples where the ion irradiation did not induce any relevant ferromagnetic contribution. This state is neither pure paramagnetic nor superparamagnetic. Phenomenologically speaking, its temperature dependence resembles that obtained from the mean-field theory where a "molecular" field proportional to the magnetization is included as well as a "critical" temperature $T^{\star}$ above which this magnetic contribution vanishes.

ACKNOWLEDGMENTS

We gratefully acknowledge the collaboration and support from D. Spemann and T. Butz, and discussions with M. Ziese. M.A.R. thanks Nuria Gordillo for her help with SRIM simulations. This work was supported by the Deutsche Forschungsgemeinschaft under Grant No. DFG ES 86/16-1, by the Spanish Ministry of Science under the program CONSOLIDER Nanociencia Molecular (Grant No. CSD2007-00010) and the Project No. MAT2008-06517-c02-01, and by the DAAD under Grant No. D/07/13369 "Acciones Integradas Hispano-Alemanas."

*miguel.ramos@uam.es
†esquin@physik.uni-leipzig.de

[1] J. F. Ziegler, *The Stopping and Range of Ions in Matter* (Pergamon Press, New York, 1977).
[2] J. F. Ziegler, J. P. Biersack, and M. D. Ziegler, SRIM—The Stopping and Range of Ions in Matter (SRIM Co., 2008), ISBN 0-9654207-1-X. See also the simulation software IIS available at http://www.ele.uva.es/jesman/iis.html, which has some advantages in comparison with the usual SRIM simulation.
[3] B. T. Kelly, *Physics of Graphite* (Applied Science, London, 1981).
[4] P. O. Lehtinen, A. S. Foster, A. Ayuela, A. Krasheninnikov, K. Nordlund, and R. M. Nieminen, Phys. Rev. Lett. **91**, 017202 (2003).
[5] Y. Ma, P. O. Lehtinen, A. S. Foster, and R. M. Nieminen, New J. Phys. **6**, 68 (2004).
[6] E. Castro, M. Löpez-Sancho, and M. Vozmediano, New J. Phys. **11**, 095017 (2009).
[7] L. Pisani, B. Montanari, and N. Harrison, New J. Phys. **10**, 033002 (2008).
[8] Y. Zhang, S. Talapatra, S. Kar, R. Vajtai, S. K. Nayak, and P. M. Ajayan, Phys. Rev. Lett. **99**, 107201 (2007).
[9] O. V. Yazyev, Phys. Rev. Lett. **101**, 037203 (2008).
[10] W. Li, M. Zhao, Y. Xia, R. Zhang, and Y. Mu, J. Mater. Chem. **19**, 9274 (2009).
[11] P. Esquinazi, D. Spemann, R. Höhne, A. Setzer, K.-H. Han, and T. Butz, Phys. Rev. Lett. **91**, 227201 (2003).
[12] J. Barzola-Quiquia, P. Esquinazi, M. Rothermel, D. Spemann, A. Setzer, and T. Butz, Nucl. Instrum. Methods Phys. Res. B **256**, 412 (2007).
[13] J. Barzola-Quiquia, P. Esquinazi, M. Rothermel, D. Spemann, T. Butz, and N. García, Phys. Rev. B **76**, 161403(R) (2007).
[14] H. Xia *et al.*, Adv. Mater. **20**, 4679 (2008).
[15] X. Yang, H. Xia, X. Qin, W. Li, Y. Dai, X. Liu, M. Zhao, Y. Xia, S. Yan, and B. Wang, Carbon **47**, 1399 (2009).
[16] P. Esquinazi, J. Barzola-Quiquia, D. Spemann, M. Rothermel, H. Ohldag, N. García, A. Setzer, and T. Butz, J. Magn. Magn. Mater. **322**, 1156 (2010).
[17] H. Ohldag, T. Tyliszczak, R. Höhne, D. Spemann, P. Esquinazi, M. Ungureanu, and T. Butz, Phys. Rev. Lett. **98**, 187204 (2007).
[18] H. Ohldag, P. Esquinazi, E. Arenholz, D. Spemann, M. Rothermel, A. Setzer, and T. Butz, arXiv:0905.4315 (unpublished).
[19] E. J. Duplock, M. Scheffler, and P. J. D. Lindan, Phys. Rev. Lett. **92**, 225502 (2004).
[20] M. Dubman *et al.*, J. Magn. Magn. Mater. **322**, 1228 (2010).
[21] X. Pei, X. Yang, and J. Dong, Phys. Rev. B **73**, 195417 (2006).
[22] K. Schindler, N. García, P. Esquinazi, and H. Ohldag, Phys. Rev. B **78**, 045433 (2008).
[23] K. W. Lee and C. E. Lee, Phys. Rev. Lett. **97**, 137206 (2006).
[24] K. W. Lee, H. Kweon, J. J. Kweon, and C. E. Lee, J. Appl. Phys. **107**, 044302 (2010).
[25] P. Reichart *et al.*, Nucl. Instrum. Methods Phys. Res. B **249**, 286 (2006).
[26] W. Anwand, G. Brauer, D. Grambole, A. Setzer, and P. Esquinazi (unpublished).
[27] F. Agullo-Lopez, C. R. A. Catlow, and P. D. Townsend, *Point Defects in Materials* (Academic Press, London, 1988).
[28] For a wide overview of the field see, for instance, *Proceedings of the 16th International Conference on Ion Beam Modification of Materials*, Dresden, Germany, 2008, edited by W. Möller and B. Rauschenbach [Nucl. Instrum. Methods Phys. Res. B **267**, 1217 (2009)].
[29] F. Banhart, Rep. Prog. Phys. **62**, 1181 (1999).
[30] M. Dresselhaus and R. Kalish, *Ion Implantation in Diamond, Graphite and Related Materials* (Springer-Verlag, Berlin, 1992).
[31] R. H. Telling and M. I. Heggie, Philos. Mag. **87**, 4797 (2007).
[32] Z. Tang, M. Hasegawa, T. Shimamura, Y. Nagai, T. Chiba, Y. Kawazoe, M. Takenaka, E. Kuramoto, and T. Iwata, Phys. Rev. Lett. **82**, 2532 (1999).
[33] J. P. Biersack and W. Eckstein, Appl. Phys. A **34**, 73 (1984); **37**, 95 (1985).
[34] A. Climent-Font, F. Pászti, G. García, M. T. Fernández-Jiménez, and F. Agulló, Nucl. Instr. and Meth. B **219-220**, 400 (2004).
[35] N. W. Ashcroft and N. D. Mermin, *Solid State Physics* (Holt-Saunders International Editions, Philadelphia, 1981), p. 653.
[36] P. O. Lehtinen, A. S. Foster, Y. Ma, A. V. Krasheninnikov, and R. M. Nieminen, Phys. Rev. Lett. **93**, 187202 (2004).
[37] K. H. J. Buschow and F. R. de Boer, *Physics of Magnetism and Magnetic Materials* (Kluwer Academic/Plenum, New York, 2003), p. 16.
[38] W. Doring, Z. Naturforscher **16a**, 1008 (1961).
[39] A. P. Levanyuk and N. García, J. Phys. Condens. Matter **4**, 10277 (1992).
[40] P. A. Serena, N. García, and A. P. Levanyuk, Phys. Rev. B **47**, 5027 (1993).
[41] J. Barzola-Quiquia, P. Esquinazi, A. Setzer, M. Ziese, M. Rothermel, D. Spemann, and T. Butz (unpublished).
[42] Y. Hishiyama, S. Yasuda, A. Yoshida, and M. Inagaki, J. Mater. Sci. **23**, 3272 (1988).
[43] K.-H. Han, P. Esquinazi, M. Diaconu, H. Schmidt, D. Spemann, and T. Butz, J. Korean Phys. Soc. **48**, 1427 (2006).
[44] P. Esquinazi, A. Setzer, R. Höhne, C. Semmelhack, Y. Kopelevich, D. Spemann, T. Butz, B. Kohlstrunk, and M. Lösche, Phys. Rev. B **66**, 024429 (2002).
[45] Y. Virmani, J. Zimbrick, and E. Zeller, Carbon **10**, 613 (1972).
[46] O. V. Yazyev and L. Helm, Phys. Rev. B **75**, 125408 (2007).
[47] K. Niwase, Phys. Rev. B **52**, 15785 (1995).
[48] G.-D. Lee, C. Z. Wang, E. Yoon, N.-M. Hwang, D.-Y. Kim, and K. M. Ho, Phys. Rev. Lett. **95**, 205501 (2005).
[49] A. Arndt, D. Spoddig, P. Esquinazi, J. Barzola-Quiquia, S. Dusari, and T. Butz, Phys. Rev. B **80**, 195402 (2009).
[50] T. Stauber, N. M. R. Peres, and F. Guinea, Phys. Rev. B **76**, 205423 (2007).
[51] I. A. Luk'yanchuk and Y. Kopelevich, Phys. Rev. Lett. **93**, 166402 (2004).
[52] J. R. Hahn, H. Kang, S. Song, and I. C. Jeon, Phys. Rev. B **53**, R1725 (1996).
[53] J. R. Hahn and H. Kang, Phys. Rev. B **60**, 6007 (1999).
[54] M. M. Ugeda, I. Brihuega, F. Guinea, and J. M. Gomez-Rodriguez, Phys. Rev. Lett. **104**, 096804 (2010).
[55] P. Ruffieux, O. Gröning, P. Schwaller, L. Schlapbach, and P. Gröning, Phys. Rev. Lett. **84**, 4910 (2000).
[56] S. Bedanta and W. Kleemann, J. Phys. D **42**, 013001 (2009).
[57] R. Höhne, K.-H. Han, P. Esquinazi, A. Setzer, H. Semmelhack, D. Spemann, and T. Butz, J. Magn. Magn. Mater. **272-276**, E839 (2004).